

AN ADAPTIVE COMPLEX INDEPENDENT COMPONENT ANALYSIS TO ANALYZE DYNAMIC CONTRAST ENHANCED-MRI

Hatef Mehrabian ^{*1}, Ian Pang¹, Rajiv Chopra¹ and Anne L. Martel¹

¹Department of Medical Biophysics, University of Toronto, Toronto, ON, Canada

ABSTRACT

Pharmacokinetic (PK) modeling of tumors provides information about perfusion and vascular permeability of tumors. Identifying arterial input function (AIF) is crucial in PK modeling using dynamic contrast enhanced (DCE)-MRI. An adaptive complex independent component analysis method is developed to identify and separate AIF from complex DCE-MRI data. The results are compared with a previously introduced AIF estimation method that applied ICA to magnitude DCE-MRI data. Using simulation and experimental phantom studies it is shown that using both magnitude and phase data (complex) results in a more robust and more accurate AIF measurement algorithm.

Index Terms— Adaptive Complex ICA (AC-ICA), Pharmacokinetic modeling, Arterial Input Function (AIF)

1. INTRODUCTION

Advances in our understanding of cancer biology have enabled clinicians to tailor treatments to individual patients. Given the specificity and cost of these treatments, proper selection of patients who would benefit from these treatments and the ability to determine tumor response to treatment early is essential to adjust the course of treatment [1]. Currently, imaging measurements of tumor size and evaluation of serum markers are the two main approaches used clinically to assess therapeutic response. However, these criteria cannot be used for all tumors as only a few tumors produce detectable markers and several molecular targeted agents result in no significant change in tumor size while showing improved clinical outcome [2]. Thus, there is significant interest in functional imaging techniques such as dynamic contrast enhanced (DCE)-MRI to develop novel metrics.

A DCE-MRI study, which involves intravenous administration of a contrast agent followed by repeated imaging to track its passage through tumor vasculature into the extravascular extracellular space (EES), provides information about blood volume and tumor microvascular permeability. Parameters extracted using pharmacokinetic (PK) modeling from DCE-MRI studies have been found to be related to prognostic factors [3] and their role in assessing anti-angiogenic therapies is increasing [4].

A fundamental step in PK modeling is determining the contrast agent concentration in the intravascular space (arterial input function) [5]. This signal is usually

inseparable from the EES contrast concentration due to partial volume effect, heterogeneous tumor vasculature and low resolution of images that makes finding purely intravascular areas in the tumor extremely difficult [6].

There is no method to directly measure the actual arterial input function (AIF) inside the tumor in these studies. To estimate the AIF, it is common to use the contrast agent concentration in an artery that is anatomically adjacent to the tumor, a standard AIF [7], a population-averaged AIF or a reference tissue based AIF [8]. There is a need for more sophisticated image processing techniques to measure the AIF.

An ICA-based method was developed to measure and separate AIF inside the tumor [9]. Although the output of MR imaging is a complex-valued, in this study (as is common in most DCE-MRI studies) only the magnitude data was used and the phase information was not utilized. This introduced a fundamental challenge in ICA analysis as the linear mixture assumption that is core to ICA was violated. This problem was addressed by using short echo time (TE) and minimizing intravoxel dephasing [9].

A more effective way of addressing the problem of intravoxel dephasing is analyzing the complex data rather than the magnitude data. In this study a complex ICA approach that complies with the linear mixture assumption of ICA is used to measure AIF. A second problem is that the choice of cost function in ICA varies as the sources may be supergaussian or subgaussian and in case of complex sources, they can be circular and non-circular. Thus using methods that assume a fixed probability density function (pdf) for both intravascular (AIF) and EES (as is common in classic ICA approaches) [9] is not optimal. An adaptive pdf is employed in ICA here and its parameters are optimized by performing on-line density estimation at each iteration.

Simulation and experimental tissue mimicking phantom studies are conducted to demonstrate the performance of complex ICA with an adaptive pdf (AC-ICA) compared to the previously introduced magnitude ICA (ICA applied to magnitude data in DCE-MRI) with a fixed cost function.

2. THEORY AND METHODS

2.1. Complex ICA with adaptive nonlinearity

Independent component analysis (ICA) is a statistical signal processing approach that aims to extract underlying features of the dataset (unobserved components or source signals) from observed mixtures such that the extracted features are

mutually independent, without assuming any knowledge of the mixing coefficients [10]. The linear mixture ICA model is expressed as $Z = AS$, where $Z = [z_1, z_2, \dots, z_N]^T$ the DCE-MRI dataset (observed mixtures), $S = [s_1, s_2, \dots, s_M]^T$ is a matrix containing the M structures that are known as independent components or ICs (usually $M \leq N$) and $A \in \mathbb{R}^{N \times M}$ is the mixing matrix. The aim of ICA is to estimate the independent components S and the mixing matrix A having the observed mixture signals Z . Classical ICA algorithms try to find an unmixing matrix $W \in \mathbb{R}^{M \times N}$ and estimate the IC matrix $Y = [y_1, y_2, \dots, y_M]^T$ such that $Y = WZ$ where rows of Y are statistically independent. The IC's can be recovered up to scaling and permutation [11].

Based on the central limit theorem, the distribution of a sum of independent random variables tends towards a Gaussian distribution [12]. Thus, to find the independent components, one has to maximize the non-Gaussianity of the extracted components. It was shown that the problem of maximizing nongaussianity translates into the following [13]:

$$w_{optimum} = \underset{\|w\|=1}{argmax} \{E\{|G(w^H Z)|^2\}\} \quad (1)$$

where H is hermitian transform, $Z = z^R + iz^I$ is the complex data and $G(Z) = -\log(p(z^R, z^I))$ where p is the joint probability distribution of z^R, z^I . The fixed point update for w derived from a quasi-Newton approach is [14]:

$$w_{k+1} = -E\left\{G^*(w^H Z)G'(w^H Z)X\right\} + E\left\{G'(w^H Z)G'^*(w^H Z)\right\}w_k + E\{XX^T\}E\left\{G^*(w^H Z)G''(w^H Z)\right\}w_k^* \quad (2)$$

The adaptive nonlinearity was chosen based on the fact that generalized normal distributions (3) cover a wide range of symmetric distributions (sub-Gaussian for $\beta < 2$ and super-Gaussian for $\beta > 2$).

$$p_y(y) = \frac{\beta}{2\alpha\Gamma(1/\beta)} \exp\left(-\frac{|y|^\beta}{\alpha^\beta}\right) \quad (3)$$

The two parameters of this pdf were calculated by finding the maximum likelihood estimate for α :

$$\alpha = \left(\frac{\beta \sum_{i=1}^N |y_i|^\beta}{N}\right)^{1/\beta} \quad (4)$$

where N is the the number of elements of y and applying the unit variance condition for sources in ICA [15]

$$E\{y^2\} = \int_0^\infty y^2 p(y) dy = \frac{\alpha^2 \Gamma(3/\beta)}{\Gamma(1/\beta)} = 1 \quad (5)$$

Starting with an initial guess for p , the two parameters are estimated by iteratively optimizing (4) and (5) and function $G(.)$ is derived as: $G(Z) = -\log(p(z^R, z^I)) = \left(\frac{z}{\alpha}\right)^\beta$

2.2 Simulation Study

A simulation study was developed to simulate DCE-MRI data of a leaky phantom (next section) using a combination of finite element analysis (FEA) and classical description of MRI physics by means of Bloch equations. The simulation phantom geometry and material properties, its MRI acquisition parameters and the concentration of contrast agent inside tubes were chosen to be close to those used in the physical phantom study in order to enable comparison.

The FEA was used to model diffusion of contrast agent from the intravascular space (tubes) to extravascular space (gel), as a bolus of contrast agent passes through the tubes. The Bloch equation simulation was performed for each voxel to generate its MR signal using the contrast agent concentration, the material properties and MRI acquisition parameters based on the algorithm presented in the SIMRI project [16]. It was assumed there are 2 spin isochromates in every voxel corresponding to water and gel to allow intravoxel dephasing. Thus, the Bloch equation was solved twice for each voxel and the water/gel content of each voxel and their contrast concentration were derived from FE analysis. The phantom consisted of a grid of 4×4 leaky tubes (internal diameter of $200\mu\text{m}$ and center to center spacing of $400\mu\text{m}$) though which water flowed with a constant rate, embedded in agar gel (imaging parameters and phantom specification explained in section 2.3).

Dynamic contrast-enhanced image simulation was performed under B_0 magnetic field of 1.5T with 1ppm inhomogeneity using a single coil RF pulse. 2D SPGR acquisition of 90 frames (temporal resolution = 3.3s) were simulated. The simulated DCE-MRI data was reconstructed in four different resolutions to highlight the performance of the proposed AIF measurement technique (AC-ICA) compared to magnitude ICA (Mag-ICA). They also demonstrate the robustness of the ICA technique in separating AIF in different resolutions, particularly in low resolutions that are more commonly encountered in clinical trials. The high resolution dataset has in-plane resolution of $150\mu\text{m}$, in other datasets high frequency elements are removed and the low resolution datasets have in-pane resolution of $300\mu\text{m}$, $600\mu\text{m}$ and $800\mu\text{m}$. A sample frame of each dataset is shown in figure 1.

2.3 Tissue Mimicking Phantom

A physical phantom was constructed that consisted of a chamber of agar gel (0.5 wt%, Sigma-Aldrich Canada Ltd., Canada) used as tissue mimicking material, through which a grid of 10×10 dialysis tubing (Diapes PES-150, Baxter, ID = $200\mu\text{m}$, wall thickness = $30\mu\text{m}$) with center to center spacing of $300\mu\text{m}$ between the tubes. These tubes path through the agar gel parallel to each other and represent the microvessels. They approximate the diameter of small arteries or large arterioles. These porous tubes (pore size of 89nm to 972nm) allow low-molecular weight contrast agent to freely diffuse from the tubes into the gel.

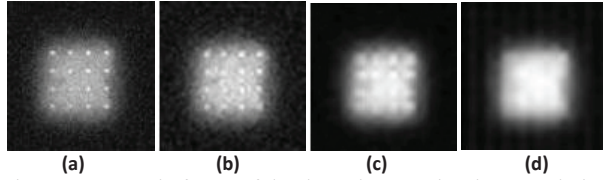


Figure 1 A sample frame of the three datasets, in-plane resolution of a) 150µm, b) 300µm c) 600µm and d) 800µm.

Dynamic contrast-enhanced imaging was performed using a 2D fSPGR acquisition (TR = 12.5 ms, TE = 2.9 ms, Flip Angle= 20, BW= 15.63 kHz, Nx/Ny/NEX = 256/256/1, FOV = 45 mm, Slice Thickness = 5 mm) where 90 images were acquired over about 4.8 minutes with a temporal resolution of 3.3 s and no delay between acquisitions. The data was reconstructed in two different resolutions: high-resolution data with in-plane resolution of 170µm and low resolution with in-plane resolution of 700µm. A sample frame of each dataset is shown in figure 2b and 2c.

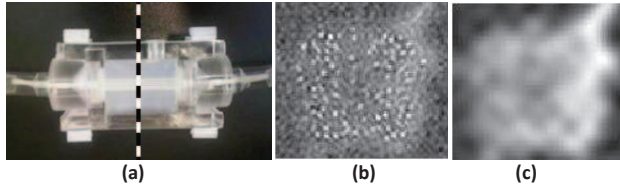


Figure 2 a) the physical phantom. Imaging is performed across the dashed line in the middle of the phantom, in a plane perpendicular to view that is shown here. a sample frame of b) high resolution and c) low resolution DCE-MRI data of experimental phantom.

3. RESULTS

3.1 Simulation Phantom study

The adaptive complex ICA as well as magnitude ICA introduced in [9] were applied to all four simulated datasets and the signal from inside the tubes (AIF) was extracted. The AIF component images for all datasets are shown in figure 3a, 3b, 3c and 3d and their corresponding intensity-time curves as well as the actual AIF curve are shown in figure 3e. As the actual amplitude of the AIF intensity-time curve is not required in the PK models and they only use their relative values, the intensity-time curves are normalized with respect to their maximum and the pre-contrast concentrations are corrected for in order to enable comparison. In figure 4 the extracted AIF IC's and their corresponding intensity-time curves for all four simulated datasets and the original AIF curve are shown for Mag-ICA.

Five DCE-MRI data of the simulation phantom with SNR=20 was generated. The analysis was performed with both ICA algorithms and in all 4 resolutions. Table 1 reports the mean squared error (MSE) between the estimated AIF curves and the actual curve for all 4 datasets using both ICA algorithms. Table 1 also reports the correlation coefficient between the estimated and actual curves.

3.2 Experimental Phantom Study

The adaptive complex ICA and magnitude ICA were also applied to DCE-MRI images of the tissue mimicking

phantom. Preliminary results of applying the two ICA algorithms to the experimental phantom data is depicted in figure 5a and 5b. These figures show the AIF curves estimated in both datasets by the two algorithms.

Table 1 mean squared error (MSE) and correlation coefficient between the estimated AIF curves and the actual curve for 4 dataset in both ICA algorithms

In-plane Resolution	150µm	300µm	600µm	800µm
Mean Squared Error				
AC-ICA	0.025±0.001	0.03±0.005	0.047±0.01	0.087±0.05
Mag-ICA	0.059±0.001	0.09±0.001	0.21±0.006	0.27±0.002
Correlation Coefficient				
AC-ICA	0.995	0.994	0.989	0.972
Mag-ICA	0.992	0.98	0.877	0.802

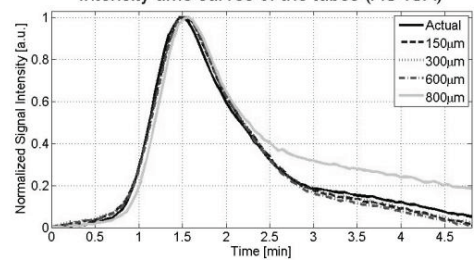
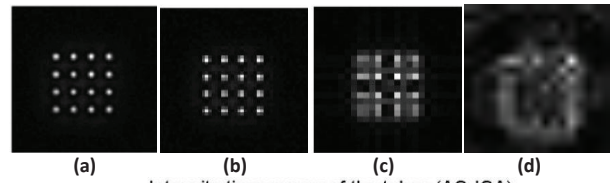


Figure 3 AIF that resulted from applying adaptive complex ICA to the 4 datasets: in-plane resolution of a) 150µm, b) 300µm, c) 600µm, d) 800µm. e) AIF curves corresponding to the 4 datasets.

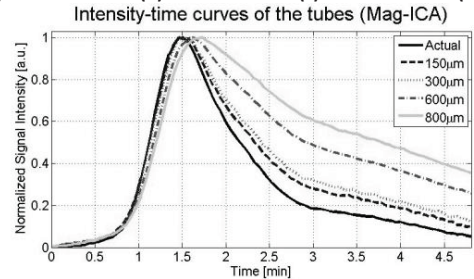
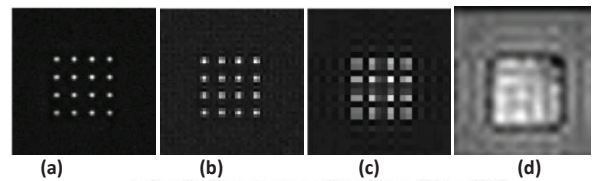


Figure 4 AIF that resulted from applying magnitude ICA to the 4 datasets: in-plane resolution of a) 150µm, b) 300µm, c) 600µm, d) 800µm. e) AIF curve corresponding to the 4 datasets.

4. DISCUSSIONS

A simulation study and an experimental phantom study were conducted to assess the feasibility of identifying and separating AIF (tubes) in DCE-MRI using ICA. An adaptive complex ICA approach was used here and was compared to magnitude ICA approach that was previously introduced. Both experimental and simulation data were reconstructed in different resolutions to assess the robustness of the method and its capability in separating AIF in low resolution data that are more common in clinical practice.

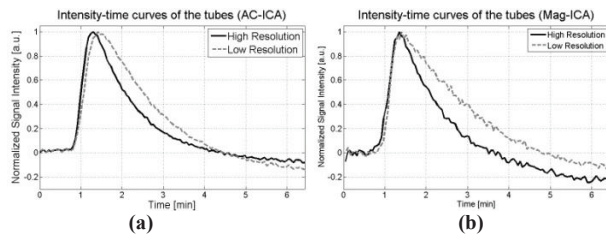


Figure 5 The AIF separated by applying a) AC-ICA and b) Mag-ICA to both datasets

As shown in figure 3e, 4e, 5c and 5d and table 1, both ICA methods were capable of separating AIF with high accuracy for high resolution data. However, AC-ICA demonstrated higher accuracy and robustness compared to magnitude ICA as the resolution of data was reduced.

There are two reasons for superior performance of AC-ICA: 1) the ICA cost function is adapted at every iteration to match the pdf of the source signal, 2) unlike the Mag-ICA, the linear mixture assumption of ICA is not violated in AC-ICA and thus intravoxel dephasing (spins inside each voxel are not necessarily in-phase) and partial volume effect do not play as significant role as they do in Mag-ICA.

It was also shown that although the tubes were not visible in the IC images of low resolution datasets (both simulation and experiment), the AIF curves in low resolution datasets are very close to the high resolution ones. This demonstrates that ICA based AIF measurement has the potential to be used in clinical studies, where the resolution of DCE-MRI data is very low.

5. CONCLUSIONS

Measuring tumor size and measuring serum markers are not efficient criteria in assessing tumor response to therapy particularly in anti-angiogenic therapies. PK analysis of DCE-MR images of the tumor provides useful information such as vascular permeability and blood volume. Measuring AIF is a fundamental step in PK analysis.

An adaptive complex ICA method was introduced to separate AIF from data and was compared to previously introduced magnitude ICA. Simulation and experimental studies were conducted and AIF was extracted with good accuracy. Although the tubes were not visible in IC images for low resolution datasets, the AIF curves in both simulation and experimental study demonstrated that AC-ICA has superior performance and showed higher stability in dealing with low resolution datasets compared to

magnitude ICA. Thus, AC-ICA has the potential to be used for AIF measurement in PK analysis of tumors on clinical studies that have very low resolution.

6. REFERENCES

- [1] H.C. Lee, *et al.* "Hepatic tumor response evaluation by MRI". *NMR Biomed* 24:721-733, 2011.
- [2] A. Forner, *et al.* "Evaluation of tumor response after locoregional therapies in hepatocellular carcinoma: Are response evaluation criteria in solid tumors reliable?" *Cancer* 115:616-623 2009.
- [3] M. Kanematsu, *et al.* "Expression of vascular endothelial growth factor in hepatocellular carcinoma and the surrounding liver and correlation with MRI findings". *Am J Roentgenol* 184:832-841, 2005.
- [4] M.O. Leach, *et al.* "Assessment of antiangiogenic and antivascular therapies in early-stage clinical trials using magnetic resonance imaging: issues and recommendations" *British Journal of Cancer* 92:1599-1610, 2005.
- [5] H.L.M. Cheng, "Investigation and optimization of parameter accuracy in dynamic contrast-enhanced MRI" *Journal of Magnetic Resonance Imaging* 28:736-743, 2008.
- [6] A. E. Hansen, *et al.* "Partial Volume Effect (PVE) on the Arterial Input Function (AIF) in T-1-Weighted Perfusion Imaging and Limitations of the Multiplicative Rescaling Approach" *Mag. Res. Med.* 62:1055-1059, 2009.
- [7] R. Lawaczeck, *et al.* "Pharmacokinetics of Contrast Media in Humans Model With Circulation, Distribution, and Renal Excretion", *Invest Radiol* 46:576-585, 2011.
- [8] X. Fan, *et al.* "Use of a Reference Tissue and Blood Vessel to Measure the Arterial Input Function in DCEMRI" *Mag. Res. Med.* 64:1821-1826, 2010.
- [9] H. Mehrabian, *et al.* "Automatic mask generation using independent component analysis in dynamic contrast enhanced-MRI", *Proc. ISBI*, 2011.
- [10] P. Comon, "Independent component analysis, A new concept?" *Signal Process* 36:287-314, 1994.
- [11] N. A. Thacker, *et al.* "Voxel based analysis of tissue volume from MRI data," *Br. J. Radiol.*, vol. 77, 2004.
- [12] A. Araujo, E. Giné "The central limit theorem for real and Banach valued random variables", NY: Wiley, 1980.
- [13] H. Mehrabian *et al.* "A constrained independent component analysis technique for artery-vein separation of TPLSM images of the cerebral microvasculature" *Med Image Anal.*, In Press 2011.
- [14] M. Novey, T. Adali, "Complex ICA by Negentropy Maximization" *IEEE TNN*, VOL. 19, NO. 4, APRIL 2008.
- [15] M. Novey, T. Adali, "Adaptable Nonlinearity for Complex Maximization of Nongaussianity and a Fixed-Point Algorithm," *Machine Learning for Signal Processing*, Proc.16th IEEE Sig. Proc. Society Workshop pp79-84, 2006.
- [16] H.B. Cattin, *et al.* "The SIMRI project: a versatile and interactive MRI simulator", *J Mag. Res.* 173 97-115, 2005.